Biomimetic mesoporous vectors enabling the efficient inhibition of wild-type isocitrate dehydrogenase in multiple myeloma cells

Biomimetic mesoporous vectors enabling the efficient inhibition of wild-type isocitrate dehydrogenase in multiple myeloma cells

Valentina Cauda[1,*], Teng Teng Xu[2], Inês Nunes[1], Elisabetta Mereu[2], Simona Villata[1], Elisa Bergaggio[2], María Labrador[2], Tania Limongi[1], Francesca Susa[1], Angelica Chiodoni[3], Michela Cumerlato[2], Giada Rosso[1], Rachele Stefania[2], Roberto Piva[2]*

[1] *Department of Applied Science and Technology, Politecnico di Torino, Corso Duca degli Abruzzi 24, 10129, Turin, Italy.*

[2] *Department of Molecular Biotechnology and Health Sciences, University of Torino, via Nizza 52, 10126, Turin, Italy.*

[3] *Istituto Italiano di Tecnologia, Center for Sustainable Future Technologies, Via Livorno 60, 10144, Turin, Italy.*

***** *Correspondence: valentina.cauda@polito.it Tel.: +39 0110907389, Fax: +39 0110907301, roberto.piva@unito.it; Tel: +39 0116334481.*

Received: date; Accepted: date; Published: date

Abstract:

The discovery of isocitrate dehydrogenases (IDHs) mutations in several malignancies has brought to the approval of drugs targeting IDH1/2 mutants in cancers. More recently it has been suggested that the enzymatic inhibition of IDHs may have therapeutic potentials also for wild-type IDH cancers. Specifically, IDH2 inhibition can sensitize multiple myeloma cells to proteasome inhibitors. However, inhibitors directed against native IDHs are not present on the market. Here, we exploited an allosteric inhibitor of mutant IDH2 (AGI-6780), known to also decrease the activity of wild-type IDH2. Since AGI-6780 effectiveness in vivo is limited by its high hydrophobicity and very low bioavailability, the drug was loaded into mesoporous silica nanoparticles (MSNs) with the aim to enhance its efficacy. Furthermore, to enable high drug retention into the silica pores, improve biocompatibility, and reduce the off-target delivery of the drug, a Supported phosphoLipidic Bilayer (SLB) was self-assembled on the outer MSN surface. The silica nanoparticles were thus coated with

three different lipid formulations and characterized in terms of structure, size, and morphology. We demonstrated that MSN@SLB nanoparticles have improved colloidal stability and hemocompatibility with respect to pristine MSN. We showed that MSN@SLB formulation displays an excellent loading and retention of the IDH2 inhibitor AGI-6780, with a limited drug leakage depending on the lipid formulation. Finally, we proved that AGI-6780-loaded MSN@SLB nanoparticles efficaciously inhibited the IDH2 enzymatic activity of multiple myeloma cells. Overall, this study provides a proof of concept of drug delivery to multiple myeloma cells by repurposing a neglected/dismissed drug (AGI-6780) with the use of smart nanoparticles and enabling the sensitization of multiple myeloma cells towards other possible treatments.

Keywords: mesoporous silica; supported lipid bilayers; isocitrate dehydrogenases; enzymatic inhibition; wild-type IDH inhibitors; nanoparticle drug delivery; multiple myeloma.

---

1. Introduction

The enzymes isocitrate dehydrogenases (IDHs) catalyze the oxidative decarboxylation of isocitrate, producing alpha-ketoglutarate (αKG) and CO_2 [1]. Human cells express three IDH paralogs (IDH1, IDH2, and IDH3), which differ in the catalytic mechanism, cofactor requirement, and subcellular localization. Specifically, IDH1 is situated in the cytosol and peroxisomes, whereas IDH2 and IDH3 are in the mitochondria. In recent years, IDHs mutations have been discovered in several malignancies. The mutant proteins display a new enzymatic activity, able to catalyze the NADPH-dependent reduction of αKG to D-2-hydroxyglutarate (D-2HG). The production of the oncometabolite D-2HG has a critical impact on the epigenetic cell status, affecting differentiation, metabolism, redox state, and DNA repair mechanisms [2, 3]. The discovery of the role of IDH1 and IDH2 mutations in oncogenesis has brought to the approval of drugs able to target such mutants in cancers. As a prominent example, the US Food and Drug Administration has approved the use of enasidenib (AG-221) and ivosidenib (AG-120), inhibitors of mutated IDH2 and IDH1, respectively, for the treatment of refractory or relapsed acute myeloid leukemia [4, 5].

While the role of mutated IDH1/2 genes has been deeply studied in cancers, the implication of aberrant expression of the wild-type IDHs enzymes and their role in carcinogenesis have been only partially investigated. In a recent work, aberrant expression of IDH1, IDH2, and IDH3 has been reviewed [6]. Concerning the focus of this paper, IDH2 plays a key role in cellular metabolism and acts in the tricarboxylic acid (TCA) cycle catalyzing the reversible oxidative decarboxylation of isocitrate to αKG, NAPDH, and CO_2. In addition, by providing mitochondrial NADPH, IDH2 protects cells from ROS-mediated oxidative damage, avoiding lipid peroxidation and DNA damage [1]. Therefore, given the critical role of IDH2 in mitochondrial bioenergetics, cellular stress responses and macromolecular synthesis, its inhibition is expected to impair the growth and survival of cancer cells [3]. Interestingly, aberrant expression of wild-type IDH2 has been recognized in several cancers [6-8]. Moreover, it has been reported that the inhibition of either mutated or wild-type IDH2 expressions could increase the efficacy of conventional cancer therapies, such as chemotherapy, radiotherapy, photodynamic therapy, and small molecule inhibitors [6, 9]. However, inhibitors specifically directed against wild-type IDHs are not available. Thus, one can exploit the mutant IDH2 inhibitor AGI-6780, which is known also to decrease the activity of wild-type IDH2, although less potently. The present challenge to face, however, is that AGI-6780 has previously failed the clinical translation as a free drug, owing to its very low bioavailability and high hydrophobicity *in vivo* [10]. Therefore, here we propose to use hybrid nanoparticles to encapsulate and deliver IDH2 inhibitors to tumor cells, and thus develop future combination therapies.

Among the broad scenario of drug-delivery systems, mesoporous silica nanoparticles (MSNs) offer unique properties, such as a very high porosity (1 cm^3/g) and a huge surface area (up to 1200 m^2/g), with very uniform and easily tunable pore sizes (ranging from 2 up to 15 nm) [11], which can be obtained in a hexagonal symmetry or in a worm-like structure [12-14]. MSNs, with their excellent biocompatibility and a size from 20 to 200 nm, have been broadly shown to be an ideal smart platform [15] for carrying and releasing drugs in a site-selective, controlled, and mechanized manner [16]. Importantly, the silica surface, rich of hydroxyl groups, offers not only a highly-hydrophilic nature, but also efficacious chemical anchoring sites to functional molecules [17], polymers [18], nucleic

acids [19], lipid bilayers [20], or other nanoparticles [21] able to improve the therapeutic or diagnostic capabilities of MSNs. The colloidal stability of MSN in biological media has to be strictly preserved to avoid aggregation and degradation phenomena [22], as it can negatively affect the endocytosis process and the further molecule delivery inside the tumor cells. A recent strategy was proposed by enveloping the MSN in lipidic bilayers. This nanoconstruct, also called "protocell" [23], has several advantages: besides guaranteeing the colloidal stability of MSNs, it increases the biocompatibility toward the cell surface, improves the uptake by endocytosis inside the tumor cell, and reduces off-target delivery of drugs. The lipidic bilayer offers an actionable gate-keeper [24, 25], avoiding the loss of drug loaded into the mesopores in the extracellular medium, while guaranteeing the drug delivery only intracellularly. Previous results reported so far in the literature have shown the proficient use of lipid bilayer-coated silica nanoparticles as smart nanocarriers for anticancer drugs, such as doxorubicin, paclitaxel, curcumin, irinotecan [26-28], or nucleic acids, such as mRNA or dsDNA [29, 30].

In this paper, we analyze for the first time the efficiency of MSN, coated by three different types of lipidic bilayers (MSN@SLB), to encapsulate a specific inhibitor of IDH2, i.e. the above-mentioned drug AGI-6780, with the clear purpose to reposition it for future therapeutic treatments, as this molecule has previously failed the clinical translation as a free drug. MSN@SLB nanoconstructs were fully characterized in terms of morphology, pore size, colloidal stability, and finally proposed to shuttle the IDH2 inhibitor to multiple myeloma (MM) cancer cells. MM is indeed a hematological tumor for which high doses of chemotherapeutics are requested and the risk of disease progression, drug resistance establishment and relapse are very common [31, 32]. MSN@SLB nanoconstructs were loaded with AGI-6780 and characterized for their drug uptake and retention ability, with very limited drug loss depending on the lipid formulation. Then, we demonstrated that the molecular delivery of AGI-6780 mediated by biomimetic mesoporous vectors can enable the efficient enzymatic inhibition of wild-type IDH2 in MM cells. The obtained results can thus pave the way for smart drug delivery [20] of dismissed drugs and propose their future use in combination with other anticancer molecules [9]. Specifically, we previously demonstrated that the IDH2 inhibitor AGI-6780 triggers synergistic cytotoxicity with proteasome inhibitors in MM, mantle cell lymphoma, Burkitt

lymphoma, and diffuse large B cell lymphoma cell lines, as well as in primary cells from MM patients and in mouse models of MM [9].

In this broader context, the present study provides the first proof of concept on the possibility to repurpose already developed drugs, i.e. AGI-6780, thanks to the efficient drug shuttling capability operated by smart porous and biomimetic nanoparticles, thus paving the way to new drug combination strategies to treat B-cell malignancies.

2. Materials and Methods

2.1 Synthesis of the Mesoporous Silica Nanoparticles (MSN)

To obtain MSNs, a template-assisted sol-gel self-assembly process was applied. A first solution was obtained by heating at 90 °C for 20 minutes a mixture of 14.3 g of triethanolamine (TEA, 99%, Sigma-Aldrich) and 1.92 g of tetraethyl orthosilicate (TEOS, 98%, Sigma-Aldrich) in a 100 mL polypropylene reactor without stirring. A second solution was prepared by heating at 60 °C a mixture of 2.41 mL of cetyltrimethylammonium chloride (CTAC, Sigma-Aldrich) and 21.7 mL of milli-Q water. Then, the two solutions were rapidly combined together and stirred at 500 rpm for 30 minutes. To obtain an outer surface of the silica nanoparticles functionalized with amino-propyl groups (-NH_2) for further dye labelling purposes, a 1:1 molar mixture of 21 µL of TEOS and 16 µL of (3-aminopropyl)trimethoxysilane (APTES, 98%, Aldrich) was prepared, where the molar amount corresponds to the 1% of the starting TEOS in the first solution mixture. The 1:1 mixture of TEOS and APTES was added to the reaction solution after exactly 30 minutes. The reaction was then left to stir overnight at 500 rpm at room temperature (RT) leading to a white suspension.

After that, 100 mL of ethanol (EtOH, 96%, Sigma-Aldrich) was added to the solution and then centrifuged at 10000 RCF (Relative Centrifugal Force) for 10 minutes.

Extraction of the organic template from the MSNs was performed by dispersing the pellet from the previous centrifugation in a solution containing 2 g of ammonium nitrate (NH_4NO_3, 98%, Sigma-Aldrich) in 100 mL of EtOH and heating at 90 °C for 45 minutes under reflux. After that, the MSN solution was centrifuged at 10000 RCF for 10 minutes. Then the pellet was dispersed in a solution of 10 mL of concentrated hydrochloric acid and 90 mL of ethanol and heated at 90 °C for 45 minutes

under reflux. The MSN were then separated by centrifugation at 10000 RCF for 10 minutes, washed thoroughly with ethanol and centrifuged (10000 RCF for 10 minutes) for at least three times. The pelleted MSN were finally resuspended in 15 mL ethanol and an aliquot of 500 µL was dried to measure the final concentration, which was between 13.6 mg/mL (as minimum) to maximum 18.7 mg/mL, depending on the synthesis batch, with a yeald of 18.5%±0.7 for all the synthesis performed.

Only in case of fluorescence microscopy, the MSNs, thanks to the presence of the amino-propyl functional groups, were labelled with Atto-647 NHS ester or with Atto-550 NHS ester by reacting 1 mg of MSN particles overnight in dark with 2 µg of dye in dimethylformammide, DMF.

2.2 Drug loading

To monitor the drug loading and release tests, UV-Vis absorbance spectra were collected in the range 200–800 nm by means of a microplate reader (Multiskan™ FC Microplate Photometer, from ThermoFischer Scientific, interfaced to a PC with the software SkanIt RE) using a 96-well plate quartz-glass (Hellma™, Hellma Optiks, Jena, Germany). All of the UV spectra were background-subtracted using the respective medium. AGI-6780 drug was obtained from Selleckchem (Munich, Germany). Calibration curves of AGI-6780 drug in DMSO, water and cell culture medium (RPMI-1640, Rosewell Park Memorial Institute) were first collected at 5 different concentrations (0.01 µM, 0.1 µM, 10 µM, 100 µM and 1 mM) considering the absorption peak at 283 nm. All these solutions were prepared starting from a stock solution of 10 mM AGI-6780 in DMSO. The calibration curve was built with Origin 8.5 software and fitted linearly.

For uploading the AGI-6780 drug (obtianed from Selleck Chem, München, Deutschland), 1 mg of MSNs, separated from ethanol by centrifugation, were combined with 0.4 mL of a solution AGI-6780 at 1 mM solution of drug in DMSO at 350 rpm under magnetic stirring for 1 hour. At the end of the loading time, each sample was centrifuged at 10000 RCF for 10 minutes and the supernatant was analysed in triplicates by the UV-Vis Spectrophotometer. A control AGI-6780 sample (in triplicate) containing the starting amount of drug, i.e. 1 mM in the same volume of DMSO, was used as Control Sample (CS). From the collected absorbance values, the residual drug concentration (in terms of µM) in the supernatant was calculated with the calibration curve of AGI-6780 in DMSO. The adsorbed amount in the MSN sample was evaluated as a subtraction between the absorption of

the control sample (CS) and that of the solution after drug loading, using the calibration curve to calculate the molar amount and thus the amount of uploaded drug, in terms of µg drug per mg of silica nanoparticles.

At the end of the test, the pelleted MSNs have been stored at -20 °C or immediately used.

Only for the specific formulation of MSN coated with DOPC-chol-DSPE-PEG, after AGI-6780 loading in pristine MSN, the collected supernatants were also analysed in triplicates and quantified by High Performance Liquid Chromatography (HPLC) in order to confirm the % encapsulation efficiency of drug. A Waters 2695 Alliance Separations Module with 2998 PDA detector was used. Signals were processed by Empower™ software (Waters, Milford, MA, USA). Separation was performed on a SunFire C18 3.5µm 4.6x150mm Waters column and 0.1% TFA in water (A) and 0.1% TFA in acetonitrile (B) as solvents, elution initial condition 40% B, isocratic elution 40 % B over 2min, gradient elution 40−100% B over 23 min, flow rate 1 mL/min and UV detection at 254 nm (t_R, retention time = 14 min). The injection volume was 50 µL. Calibration curves for AGI-6780 were constructed over the range from 0.6 μg $ml^{-1}$to 5 μg $ml^{-1}$of AGI-6780 in water and acetonitrile 1:1 (v/v). The limit of quantification was 0.05 μg ml^{-1}.

2.3 Biomimetic lipid bilayer formation

Three different types of lipids were prepared as biomimetic shielding of the nanoparticles. The first one was composed by DOPC (1,2-dioleoyl-sn-glycero-3-phosphocholine, 2.5 mg Avanti Polar). The second one was formulated by mixing DOPC and DOTAP (N-[1-(2,3-Dioleoyloxy)propyl]-N,N,N-trimethylammonium methyl-sulfate, Avanti Polar) at a mass percentage ratio of 70 : 30 (resulting in 1.75 mg DOPC and 0.75 mg DOTAP, i.e. a molar ratio of 2 : 1), as previously reported [20]. The third lipid composition was prepared mixing DOPC, DSPE-PEG2000-amine (1,2-distearoyl-sn-glycero-3-phosphoethanolamine-N-[polyethylene glycol-2000]-amine, Avanti Polar) and cholesterol (Sigma Aldrich) at a mass percentage ratio of 65.3: 8.6 : 26.1 (resulting in 2.5 mg DOPC, 0.33 mg DSPE-PEG2000-amine, 1.0 mg cholesterol, i.e. a molar ratio of 55 : 2 : 44, as previously reported [23]). The respective amounts of lipids were mixed in chloroform in glass vials and dried overnight in dark conditions. Afterward, the dried lipid mixtures were dissolved in 1

mL of a solution composed by 600 µL of MilliQ water and 400 µL of 99% ethanol, EtOH (where H_2O:EtOH are as 60:40 in volume). This mixture guarantees that the lipids are still dispersed as single macromolecules, preventing their assembly in liposomes. 1 mg of MSNs loaded with AGI-6780 drug or labeled by ATTO-dyes were separated by the solvent (either DMSO after drug loading or EtOH after labelling) by centrifugation at 10000 RCF for 5 minutes. The coupling between the lipids and the MSN was carried out by a solvent exchange method, as also reported in [20]. In particular, 100 µL of lipid solution, prepared as above, was added to each MSN sample, once pelleted after centrifugation. After slight pipetting, 900 µL of MilliQ water was added, obtaining the samples MSN@DOPC, MSN@DOPC:DOTAP or MSN@DOPC-chol-DSPE-PEG. In the case of fluorescent labelling, the lipophilic dye $DiOC_{18}(3)$ (3,3'-dioctadecyloxacarbocyanine perchlorate) (DiO; λ_{Ex} = 484 nm, Invitrogen, CA, USA) was also added (0.5 µl from a stock dye solution of 10 µM in DMSO) to each sample.

2.4 Samples characterization

The pristine MSNs were analysed by Fourier-Transformed infraRed (FTIR)-Spectroscopy in transmission mode to reveal their correct functionalization with amine-groups. Spectra were acquired with 4 cm^{-1} resolution and 16 scans accumulation, with a Nicolet 5700 FTIR Spectrometer (ThermoFisher, Waltham, MA, USA equipped with a RT working DLaTGS detector), and background subtracted.

The specific surface area of the pristine MSN was measured by nitrogen adsorption and desorption isotherms by using a QUADRASORB evo™ Gas Sorption Surface Area and Pore Size Analyzer instrument from Quantachrome.

Transmission Electron Microscopy (TEM) of the pristine MSN, to allow visualization of the mesopores at high resolution, was performed by a Tecnai F20ST from FEI operating at 200 kV. The samples were prepared by diluting 6 µL of MSN suspension in ultrapure absolute ethanol (99%, Sigma) with a final concentration of 100 µg/mL and drying a drop of the resulting suspension on a holey carbon-coated copper grid for TEM. With the same instrument, a Scanning Transmission Electron Microscopy (STEM) analysis was also carried out.

To analyse the MSNs size and their Zeta potential, before and after lipid bilayer formation, the nanoparticles were characterized by Dynamic Light Scattering (DLS) and Z-potential analysis with a Zetasizer Nano ZS90 (laser source He-Ne of 633 nm). Samples were measured in polystyrene disposable cuvettes for DLS and electrode-equipped and folded capillary cell cuvettes for Z-potential measurements. A volume of 1 mL was used for each samples at a concentration of 500 µg/mL either in water and ethanol, for DLS measurement, and in water for Z-potential ones.

2.5 Nanoconstruct stability over time

To investigate the effective residence time of the AGI-6780 drug in the MSN pores during the lipid bilayer formation, as well as the possible sealing effect of the different lipid bilayers over time, the nanocostruct stability was also tested in water medium only, i.e. the starting water used for the self-assembly of the lipid bilayer. The drug-loaded MSNs (0.5 mg) coated by lipids were centrifuged and transferred in 500 µL water solution, as used during lipid self-assembly in static conditions at either 4 °C or 37 °C. At selected time points, i.e. 30 min, 4 h, 24 h and 48 h, the drug-loaded particles were processed as in the drug-release experiments (see Paragraph 2.6) and the water supernatant analysed by microplate reader to collect the UV-Vis absorbance spectra of the drug. With the use of the calibration curve of AGI-6780 in water, the amount of leaked AGI-6780 was then calculated.

2.6 Drug release

The release of AGI-6780 drug was first performed in acellular media, using aliquots of 100 µg each of drug-loaded MSN@SLB nanoparticles and drug-loaded pristine MSN wihotut lipids as control. As all these samples were prepared in water medium, they were first centrifuged at 10000 RCF for 5 minutes. The water supernatant was then removed and the 100 µg sample aliquots were dispersed in 1 mL of RPMI 1640 (Pan Biotech), thus having a final concentration of MSN@SLB in RPMI of 100 µg/mL (five replicates were used for each sample type), and then placed in the orbital shaker at 37 °C and speed 200 rpm. After selected time points of 2h, 4h, 6h, 24h, 48h, 72h, 96h (4d) and 168h (7d), the samples were centrifuged (10000 RCF for 5 minutes), the supernatant was separated from the MSN@SLB to stop the drug release and three aliquots of 100 µL from the RPMI supernatant were analysed by a microplate reader. Thus, the total amount of aliquots analysed per each sample type at each time point of the release was in total 15, allowing to calculate the standard

deviation as error bar. The UV-Vis absorbance was acquired at 283 nm, according to the previous calibration curve of AGI-6780 in RPMI-1640, which was used to estimate the delivered concentration of drug in RPMI medium from the NPs.

After the reading, the aliquots were recovered and combined with their remaining supernatant and then back to each respective sample. Then the MSN@SLB were dispersed by a vortex mixer and then placed into the orbital shaker at 37 °C to further proceed with the drug release.

As controls, three samples of RPMI only (1 mL for each one) were processed in the same way as the samples containing the drug-loaded NPs and used for the background subtraction at each microplate reading.

2.7 Addition of Triton X in Drug release from MSN@SLB

To prove that the lipid coating hinders like a barrier to the drug release from the MSN, 100 μL of the surfactant Triton X-100 (Sigma-Aldrich) were added in each drug-loaded MSN@SLB at the end of the drug release experiments in RPMI-1640 medium, as already described above. It is actually expected that the surfactant would disassemble the lipid bilayer constituted on the MSN, thus promoting the release of the encapsulated drug. The analysis of the supernatants after the Triton X-100 addition was done 48 hours later, to lead enough time to the drug to out-diffuse. Then centrifugation to separate the MSN particles was operated and the analysis on the supernatant again performed by UV-Vis spectrometry at 283 nm.

2.8 Fluorescence microscopy imaging

Each sample of MSNs coupled with lipids ready after preparation (at the concentration of 1 mg/mL) was characterized through fluorescence microscopy with a co-localization method to evaluate the percentage of coupling between lipids and MSNs. Samples were prepared by withdrawing 10 μL of the lipid-coated MSN solution and depositing them on the microscope slide; then the drops were covered with a cover-glass slip and this was fixed with a common nail polish. The images were acquired using a wide-field optical fluorescence microscope Nikon Eclipse Ti, equipped with a super-bright wide spectrum Shutter Lambda XL source with a collection of four filter cubes. The images were acquired with 60x and 100x PLAN-APO immersion oil objectives and the data analyzed by the NIS-element software. MSNs were labelled with Atto-647 NHS ester or with

Atto-550 NHS ester and the lipids with $DiOC_{18}$, as described above. Images were thus acquired by exciting the dyes at two different wavelength channels: 647 nm (far-red channel) and 488 nm (green channel). The colocalization tool of NIS-Element software (NIS-Elements AR 4.5, Nikon) was used to evaluate the coupling percentages, as previously reported [20, 33, 34]: after setting a threshold between 0.1 and 1 μm to disregard larger aggregates, the spots in the red channel (identifying the MSNs) and green channels (corresponding to the lipid bilayer vesicles) were counted and an overlay of the two images was performed, counting only the spots in which the two fluorescences were colocalized. At least 10 fields of view of each sample were analyzed by this automatic routine by applying a dimensional threshold. The percentage of colocalization was then calculated with respect to the MSN channel with the following formula, Equation 2:

$$\%\text{MSNs colocalized} = (\text{n° MSNs colocalized})/(\text{n° MSNs}) \quad [\text{Eq. 2}]$$

2.9 Haemocompatibility tests

To assess nanoparticles' hemocompatibility, the plasma re-calcification time was measured following the activation of prothrombin in the presence of calcium cations (Ca^{2+}), as previously described [35-37]. Here, two identical sets of samples were prepared in citrated plasma analyzed contextually: one was treated with calcium chloride and showed coagulation, the other was left without calcium chloride and used as control. Pristine MSN and MSN@DOPC-chol-DSPE-PEG after overnight dialysis were washed twice with water and then centrifuged (10000 RCF for 5 min). Under sterile conditions, each pellet was resuspended in 1 mL of a 0.1 μm filtered physiological solution (water with 0.9% NaCl). Samples were then diluted with physiological solution to obtain two concentrations each: 100 μg/mL and 50 μg/mL. In details, a 96-well plate was prepared with 75 μL of human citrated plasma (Human Recovered Plasma Pooled-frozen – NaCitrate from ZenBio) per each well. Then, 75 μL of pure physiological solution or two different sample concentrations were added. The plate was first incubated at 37°C for 5 min, 150 μL calcium chloride (25 mM) were

quickly added and the plate was immediately read with an UV-Vis spectrometer (pre-heated at 37°C). Specifically, samples were divided in two groups: the samples (and related control solutions) treated with calcium chloride ($CaCl_2$, 25 mM) and untreated samples (each of them in triplicate). The plasma clotting protocol consists in the periodical reading of the UV absorbance of the samples at 405 nm, as a change of turbidity of the solutions of recalcified plasma due to the formation of fibrins: a measure was collected every 30 s for 45 minutes at 37 °C. The coagulation time ($\boldsymbol{t_c}$) was calculated as the time point corresponding to the central absorbance point ($\boldsymbol{a_c}$), calculated as follows: $a_c = min\ (a) + [max(a) - min(a)]/2$, where a is the vector of the UV absorbance values of the sample. Two independent experiments were carried out.

2.10 Cell cultures

Human multiple myeloma (MM) cell line KMS-28 was kindly provided by Prof. Antonino Neri (University of Milan) and authenticated by DNA fingerprinting using GenePrint system (Promega, Madison, Wisconsin, USA). Cells were maintained in RPMI 1640 medium (EuroClone, Pero, Italy), supplemented with 2 mM of L-glutamine, 100 U/mL of penicillin, 100 µg/mL of streptomycin (Gibco), 10% fetal bovine serum (FBS; Sigma-Aldrich, St. Louis, Missouri, USA), and grown at 37°C in a humidified atmosphere with 5% CO_2.

2.11 IDH enzymatic activity

To test the ability of lipid-coated nanoparticles to intracellularly release AGI-6780, IDH2 enzymatic activity was measured after 6 hours and 24 hours post treatment in mitochondrial extracts derived from KMS-28 cells previously incubated with empty and AGI-6780-loaded MSN@SLB nanoconstructs. Controls were performed treating cells with soluble AGI-6780 (5 µM), used as positive control, or left untreated (UT).

Isocitrate Dehydrogenase Activity was measured using the IDH assay kit (Sigma-Aldrich, St. Louis, Missouri, USA), according to the manufacturer's protocol. IDH activity was determined using isocitrate as a substrate of the reaction, which results in a colorimetric (450 nm) product proportional to the enzymatic activity present. One unit of IDH is the amount of enzyme that generates 1.0 µmole

of NADH or NADP per minute at pH 8.0 at 37 °C. IDH2 activity is reported as milliunit per milligram of extracted protein (mU/mg).

AGI-6780 was loaded into MSN and the lipid bilayer formulations DOPC or DOPC-chol-DSPE-PEG were self-assembled on drug loaded MSN (as reported above). Only for the MSN@ DOPC-chol-DSPE-PEG, this sample was dialyzed in 1 L Phosphate Buffer Saline (PBS) by magnetic stirring (200 rpm) for 20 hours at room temperature. The dialysis membrane had a cut-off of 3.5 K MWCO (SnakeSkin Dialysis Tubing, Thermo Scientific). MSN@SLB was then collected from the dialysis bag, centrifuged (10'000 RCF, 5 minutes), and the supernatant was analyzed by HPLC to exclude drug leakage from nanoparticles. Finally, all the drug-loaded MSN@SLB were pelleted by centrifugation and dissolved in cell culture medium and aliquoted (at 25 or 100 µg/ml) for further incubation with KMS-28 cells.

3. Results

3.1. MSNs design and characterization

To efficiently load and deliver the drug in a controlled manner, without off-target release, MSNs with a size of around 50 nm and mesoporous pore size of about 3 nm were designed and then produced. As described in the Materials and Methods section, a template-assisted sol-gel chemical synthesis was applied to obtain MSNs displaying amine-functional groups at the external nanoparticle surface. Amine groups enable the labelling of the MSNs with fluorescent dye for fluorescence microscopy studies, and allow a positively charged surface, thus increasing their z-potential, which is beneficial for the nanoparticle stability in water media.

TEM and STEM show the highly porous MSN, nanoparticles diameter of around 50 nm and pores of around 3 nm (Figure 1a and b). Mesopores have a worm-like structure, asymmetrical but highly interconnected, ideal to store high amount of drug molecules. The nitrogen sorption isotherm in Figure 1c is of Type IV, which is typical of mesoporous materials. It further confirms that the obtained MSNs have both a specific surface area (912.7 m^2/g), as evaluated by BET model, as well

as a high pore volume (around 1.185 cm^3/g) with a uniform pore size of 3 nm, as evaluated by DFT model. Such properties may guarantee a high adsorption level of the drug. FTIR in Figure 1d shows the fingerprint of silica and confirms the chemical surface functionalization with amino-propyl groups. In particular, at 1063 cm^{-1} and at 1080 cm^{-1} the -OH bond bending vibration and the characteristic peak of the silicon oxide are observed, respectively. The broad band from 3000 to 3600 cm^{-1} is related to the stretching vibrations of -OH groups, while those from 3000 to 2800 cm^{-1} are ascribed to the alkyl groups ($-CH_x$) related to the propyl chain of the APTES functional moiety. Finally, at 3700 cm^{-1} the stretching vibration related to the amine groups, grafted at the nanoparticles surface, is observed.

The MSNs size distributions in both ethanol (EtOH) and water were measured by DLS and Z-potential measurements. As reported in Figure 2.a and Table 1 (first row), these amine-functionalized nanoparticles show a moderate agglomeration, as compared with the TEM results, both in ethanol and water solutions, with a hydrodynamic diameter of 220 nm and 190 nm, respectively. They also have a polydispersed size distribution in both media, with PDI (PolyDispersive Index) of 0.83 in ethanol and 0.91 in water. The Zeta potential value is of +26 mV, accounting to the amine group protonation.

3.2 MSNs drug loading and lipid coating

Drug loading was performed on the MSN before self-assembling the lipidic bilayer, obtaining 22.2 ± 1.4 µg of loaded drug per 1 mg of silica , n=8, see Table 2, first row). Considering the molecular structure of the drug AGI-6780 (as provided by the producer, Selleckchem), the molecule displays three amine groups which can potentially establish hydrogen interactions with hydroxyl group present on the silica pore surface, thus allowing an efficient drug physisorption.

After drug adsorption, the AGI-loaded MSNs were coated by three different lipid mixtures (as detailed in the Material and Method section) to form lipid bilayers, obtaining AGI-MSN@SLB. The aim of this Supported phosphoLipidic Bilayer (SLB), self-assembled on the outer MSN surface, is to induce high drug retention of the drug molecule loaded in the silica pores and further improve the MSNs stability in water-based media. The three different lipid formulations, i.e. DOPC, DOPC-

DOTAP, and DOPC-chol-DSPE-PEG, where selected according to the previous literature related to our group [20, 33, 38, 39] for the first two formulations, while the third one was explored according to similar formulations reported in [23]. The process used to self-assemble the phospholipidic bilayers on the silica outer surface is based on the solvent exchange method, as previously reported [20, 33]. Briefly, the driving idea is to have lipid mixtures in a solution of 60 %vol. water and 40 %vol. EtOH, which guarantees that the lipids are still dispersed as single macromolecules, preventing their assembly in liposomes. Then, after being in contact with silica nanoparticles, the water content is dramatically increased, forcing the phospholipids to self-assemble as bilayers on the most energetically favoured conditions, i.e. the surface offered by the silica nanoparticles.

To prove the effective coating of SLB on the MSN, dynamic light scattering (DLS), Z-potential measurement, and co-localization fluorescence microscopy experiments were firstly run using the unloaded MSNs.

The DLS results are reported in Figure 2, showing a comparison of the hydrodynamic size distributions among the pristine MSN in water (black curves) versus the MSN@SLB (in Figures from 2b to 2d). As it can be observed, both the size distributions and the related PDIs of each MSN@SLB are lower than the pristine MSN, pointing out a fairly well-dispersed distribution peaking at 142 nm for MSN@DOPC (red curve), at 106 nm for MSN@DOPC-DOTAP (pink curve), and at 106 nm MSN@DOPC-chol-DSPE-PEG (orange curve). In contrast, both the hydrodynamic size and the related PDI of pristine MSNs show that the sample easily aggregates.

The improved stabilization of lipid-coated silica nanoparticles is also supported by the variation of the Z-Potential values (Table 1). These data confirm the coating of the nanoparticles by lipid bilayers and supporting their role as efficient steric stabilizer preventing the aggregation of MSN in water, as also previously reported [20]. In particular, the use of cationic lipids like DOTAP and DSPE-PEG, having indeed an amine terminal (DSPE-PEG2000-amine, as reported in the Materials and Method section) account for a positive value of Z-potential in water. To predict the behavior in cell culture medium, Z-potential measurements were also performed in RPMI-1640 supplemented with 10% of FBS at 37°C, which is actually the same conditions used to culture the KMS-28 cancer cells. The values (see Table 1, second column) show that all MSN@SLB nanoconstructs report a negative

Z-potential value, attributed to the adsorption of proteins on the lipid bilayer surface once immersed in the cell culture medium, also in fair agreement with the previous literature [39, 40]. The z-potential of pristine MSN was not recorded, as the material aggregates and precipitates almost immediately when in contact with the medium at 37 °C.

Further wide-field fluorescence microscopy images in Figure 3 show in the green channel (left panels) the $DiOC_{18}$-labelled phospholipids, in the red channel (middle panels) the Atto 550-labelled MSNs, and the merged channels in the right panels, demonstrating a broad level of colocalization of the dyes in all the three MSN@SLB formulations. It has to be noted that the optical resolution of wide-field fluorescence microscopy is not high enough to allow for a resolution of single MSN@SLB nanoparticles. Here, the colocalization technique is just used to support the previous characterizations and provide an estimation of the colocalization % of the two dyes. Such estimation leads to values of 24% for MSN@DOPC, 60% for MSN@DOPC-DOTAP, and 55% MSN@DOPC-chol-DSPE-PEG. These data, together with the other characterizations, in particular DLS and Z-Potential, confirm with good confidence that most of MSNs are encapsulated by the phospholipidic bilayers. The possible empty lipids nanoparticles are not relevant for the further evaluation in terms of drug encapsulation, release and cell viability experiments, as they are empty vesicles, while the drug is sealed inside the silica nanoparticles.

It has to be noted that, during the lipid self-assembly process, drug-loaded MSNs are thoroughly mixed with the lipids solution (made of 60% water and 40% EtOH, as mentioned above) for few seconds, thus a certain amount of drug is leaked out from the silica pores and dissolved in the medium before the lipid self-assembly on the silica surface. Actually, by analyzing with UV-Vis absorption the solution after the lipid self-assembly, various amounts of drug were found in solution, depending on the lipid bilayer type. The drug loss in water after immediate constitution of the lipidic bilayer was found to be relatively high, i.e. up to 21 µg per mg of silica for the sample MSN@DOPC, while less in MSN@DOPC-DOTAP samples (up to 10 µg of AGI-6780 per mg of silica) and almost zero in MSN@DOPC-chol-DSPE-PEG. The remaining amount estimated in each MSN@SLB is reported in Table 2. We hypothesize that the lipid formulation containing DOPC only is not sufficiently stable and compact to prevent the drug to leak out from the silica surface.

442

443 *3.3 MSN@SLB stability over time and release*

444 The previous results motivated us to further investigate the stability over time of the MSN@SLB
445 in water at 4 °C and 37 °C, in order to understand how long and at which conditions they can be
446 eventually stored prior to biological tests. In particular, the stability of the three nanoconstructs after
447 24 hours in water was evaluated, calculating the amount of leaked drug in water media as a function
448 of storage temperatures, i.e. 4 °C and 37 °C, before getting the nanoconstructs in contact with cell
449 cultures. Figure 4a show that the highest leakage is for sample MSN@DOPC at both temperatures,
450 followed by MSN@DOPC-DOTAP, in line with what obtained above when analyzing the solution
451 immediately after the lipid self-assembly. We observed that the DOPC-chol-DSPE-PEG lipid
452 formulation shows the best drug retention, most likely as a consequence of the fluidity impaired to
453 the lipid membrane by cholesterol, thus it can be the preferred formulation for MSN@SLB.

454

455 Preliminary drug release tests in cell culture medium in absence of cells were then conducted on
456 the AGI-loaded silica (i.e. MSN@DOPC-DOTAP and MSN@DOPC-chol-DSPE-PEG) at 37 °C in
457 RPMI-1640 medium and, as a reference, on the uncoated AGI-loaded silica nanoparticles. It has to
458 be noted that the possible drug leaked in water medium after the lipid self-assembly was discarded
459 by centrifugation and the pelleted nanoconstructs resuspended in fresh RPMI-1640 medium.

460 Figure 4b reports the progressive release of the hydrophobic drug AGI-6780 out from the pores
461 of MSN as percentage of drug released with respect to the total adsorbed amount. Concerning the
462 uncoated MSN, it is noticeable that the drug release trend increases in the first 24 hours up to 26 %
463 of the total adsorbed drug in the silica (corresponding to 6±2 μg/mg), then it remains constant until
464 72 hours of release. At last, after 5 days, the release increases sharply. At the end of the test, i.e. after
465 7 days, the release curve has not reached a plateau yet, corresponding to around 55% of the total
466 loaded drug, i.e. 12±2 μg/mg.

467 In contrast, when a lipidic bilayer is self-assembled on the MSN surface after the loading of AGI,
468 almost no drug release is observed in the cell culture medium, except for a first small burst release
469 probably due to a partial retention of drug in the outer lipid bilayer (see more details in the inset of

Figure 4b). This absence of drug release is persistent up to 7 days of daily monitoring, reaching in the worst case around 2.2% of released drug with respect to the total adsorbed amount, which corresponds to 0.3 µg/mg of AGI-6780. This result actually demonstrates that the lipid bilayer, irrespectively from its composition (DOPC-DOTAP or DOPC-chol-DSPE-PEG), is able to tightly seal the AGI-6780 inhibitor inside the silica mesopores, providing possibly a successful drug release only once internalized into cancer cells, as shown below.

After the above-reported drug release, an artificial breakage of the lipidic membrane is operated by adding Triton X-100, a surfactant well-known for its ability to disrupt the self-assembly of lipidic bilayers, as reported in [20]. Punctual release of AGI-6780 is observed reaching the average concentration of 14.6±4 µg per mg of nanoparticles in 48 hours in the releasing solution for all MSN@SLB lipid formulations yet corresponding almost to 66% of the total AGI-6780 incorporated initially in the MSN pores, or almost completely when considering the residual amount after lipid self-assembly (Table 2). Therefore, this triton-triggered release demonstrated, as previously reported in the literature [20], the effective sealing operated by the lipids and thus the ability of the whole MSN@SLB to reach intact and without drug loss the target cells.

3.4 Haemocompatibility of MSN@SLB

The haemocompatibility test consists in the evaluation of the time necessary for plasma to clot, in presence of nanoparticles. Normally, plasma is treated with anticoagulants in order to prevent clotting and allow its proper storage and employment. In the present case, we therefore used plasma citrate. The anticoagulant effect of plasma citrate was overridden by calcium chloride ($CaCl_2$) which typically induces a rapid calcification and thus clotting in about 10 minutes, with increase of turbidity. The obtained results of coagulation time in presence of pristine MSN and MSN@DOPC-chol-DSPE-PEG at two different concentrations (50 and 100 µg/ml, without drug) are reported in Figure 5 and compared to the control solutions, i.e. citrate plasma, citrate plasma with physiologic solution, and all the samples without the coagulating agent, calcium chloride. Two independent tests were conducted

(here only one is shown as representative result for both) showing notably similar results, suggesting a good repeatability of the test.

The data show a clear difference between all the control samples (not clotted, see dashed lines) and samples treated with $CaCl_2$ (clotted plasma, solid lines). Furthermore, it is worth to note that the plasma containing the MSN@SLB nanoparticles coagulates at nearly the same time (around 9.5 minutes) of the pure citrate plasma and citrate plasma together with physiological solution. In contrast, the plasma containing the uncoated MSNs samples at both concentrations coagulate earlier than the other samples, i.e. after about 4 minutes. More in details, there is a statistical significant difference between the uncoated MSNs and the lipid-coated ones at both concentrations, i.e. at 50 µg/mL (with P value equals to 0.0019) and at 100 µg/mL (P = 0.0225).

These results indicate that the lipid bilayer coating is fundamental for haematological compatibility of the proposed silica nanoparticles, as also previously reported by some of us with similar tests on polymer-coated MSNs [41]. These data can be also considered as a demonstration of the efficient and stable lipidic coating on the MSNs surface.

3.5 IDH2 enzymatic inhibition tests of AGI-6780-loaded MSN@SLB

To test the ability of the lipid-coated nanoparticles to efficiently release the IDH2 inhibitor to multiple myeloma cells, AGI-6780-loaded MSN@SLB nanoconstructs were incubated with KMS-28 cells. The effects on the mitochondrial enzyme IDH2 was then evaluated. It was decided to work with the MSN@SLB particles with either the lowest amount of loaded drug (i.e. MSN@DOPC, at a high concentration 100 µg/mL, where thus the amount of 0.3 µg of drug is calculated, according to Table 2), to look at the possible most critical or even inefficient conditions, as well as with the optimized nanoconstruct (i.e. MSN@DOPC-chol-DSPE-PEG, lowering the concentration to 25 µg/mL), which have shown the highest colloidal stability and drug retention over time. For this sample, the average amount of AGI loaded in 1 mg of MSN is estimated as 2.5 µg after the dialysis process with HPLC (see Materials and Method section), corresponding to a drug concentration in 1 mL of cell medium

of 0.13 µM (considering the nanoconstruct concentration of 25 µg/mL used in this enzymatic inhibition test) .

Table 3 shows the results of enzymatic inhibition after 6 and 24 hours calculated as the inhibition percentage of drug-loaded MSN@SLB with respect to the control, i.e. MSN@SLB constructs without drug. The data also displays the enzymatic activity inhibition in cells treated with the drug dissolved at a concentration of 5 µM in the cell medium with respect to the untreated cells.

While untreated and MSN@SLB-treated cells did not display any enzymatic activity inhibition, both AGI-6780-loaded MSN@SLB nanoconstructs inhibited IDH2 activity in a time-dependent manner. It is worth noting that drug-loaded MSN@DOPC and MSN@DOPC-chol-DSPE-PEG slightly affect the endogenous IDH2 activity at 6 hours, while this inhibition increases after 24 hours. As a positive control, 5 µM AGI-6780 dissolved in the cell culture medium showed a comparable but higher enzymatic inhibition. This is known to occur in in-vitro tests [9], while in-vivo data or further clinical translation for the free AGI-6780 could not be obtained for its low solubility and short half-life in liver microsomes [10]. Therefore, the contribution of the here proposed nanoconstructs, able to carry efficiently the drug and deliver it intracellularly, is a valuable option for further in-vivo and clinical translations.

It is worth to note that these experiments are just a proof of the principle, but they already confirm not only the efficacy of AGI-6780 as a wild-type IDH2 inhibitor, but also that the drug is efficiently delivered to cells by the formulated nanoconstructs and a low amount of nanocarried drug is thus sufficient to induce a consistent enzymatic inhibition.

It has to be also pointed out that AGI-6780 is not per se cytotoxic at concentrations that specifically inhibit IDH2 activity. Therefore, its clinical relevance could be detectable only in combinations with other drugs, such as chemotherapeutics or proteasome inhibitors [6]. In particular, we have previously shown that wild type IDH2 inhibition sensitizes B-cell malignancies to proteasome inhibitors [9]. Based on this previous knowledge, the current results open the way to new possible nanotechnological strategies, enabling the synergistic treatment of nanocarried IDH2 inhibitor with chemotherapeutics or proteasome inhibitors.

5. Conclusions

In the present study, we have described the preparation of mesoporous silica nanoparticles shielded by various formulations of lipid bilayer coatings to be used efficiently as drug delivery vehicles. The colloidal stability, the haemocompatibility, the efficient drug loading and release capabilities of such nanoconstruct were demonstrated. Specifically, we have shown that porous nanocarriers loaded with the IDH2 inhibitor AGI-6780 are suitable vectors for efficient drug retention and cancer cell delivery. Furthermore, we have demonstrated that such drug-loaded nanoconstruct could successfully inhibit wild-type IDH2 enzymatic activity in multiple myeloma cells.

Our study provides a proof-of-concept instrumental to reposition unapproved drugs and to propose their therapeutic use through nanocarrier administration. We suggest that inhibition of wild-type IDH2 can become a potential therapeutic option for synergistic treatments in multiple myeloma aimed at sensitizing drug-resistant cancer cells. Future studies will focus on the design of nanoparticle delivery systems equipped with high-affinity ligands capable of targeting drug combinations towards cancer cells while sparing healthy tissues. In conclusion, in this paper we report a preliminary but important step toward in-vivo translation and the application of nanosized weapons in the fight against cancer and, possibly, toward other diseases.

6. Patents

A patent is already filed with research report leading to part of the work reported in this manuscript. Title:“A biomimetic nanoporous carrier comprising an inhibitor directed towards the native form of IDH2 protein” PCT: IB2020/050401 of 20th Jan. 2020 (First priority: “Vettore nanoporoso biomimetico comprendente un inibitore diretto verso la forma nativa della proteina IDH2” Italian Patent N. IT102019000001009, priority on 23rd January 2019) Inventors: V. Cauda, R. Piva, T. Limongi, L. Racca, M. Canta, F. Susa, E. Bergaggio, N. Vitale, E. Mereu.

Funding: This research was funded by AIRC Investigator Grant N. IG 21587 from the Italian Association of the Cancer Research to Prof. Roberto Piva and was carried out in the framework of the project PoC Instrument granted to Prof. Valentina Cauda by LINKS, LIFTT and Compagnia di San Paolo.

Conflicts of Interest: The authors declare no conflict of interest.

References

[1] S. Tommasini-Ghelfi, K. Murnan, F.M. Kouri, A.S. Mahajan, J.L. May, A.H. Stegh, Cancer-associated mutation and beyond: The emerging biology of isocitrate dehydrogenases in human disease, Sci. Adv., 5 (2019) eaaw4543.

[2] L.M. Gagné, K. Boulay, I. Topisirovic, M.-É. Huot, F.A. Mallette, Oncogenic Activities of IDH1/2 Mutations: From Epigenetics to Cellular Signaling, Trends Cell Biol., 27 (2017) 738–752.

[3] R.J. Molenaar, J.P. Maciejewski, J.W. Wilmink, C.J.F. van Noorden, Wild-type and mutated IDH1/2 enzymes and therapy responses, Oncogene, 37 (2018) 1949–1960.

[4] E.S. Kim, Enasidenib: First Global Approval, Drugs, 77 (2017) 1705–1711.

[5] C.D. DiNardo, Ivosidenib in IDH1-Mutated Acute Myeloid Leukemia., N. Engl. J. Med., 379 (2018) 1186.

[6] E. Bergaggio, R. Piva, Wild-Type IDH Enzymes as Actionable Targets for Cancer Therapy, Cancers, 11 (2019) 563.

[7] X. Chen, W. Xu, C. Wang, F. Liu, S. Guan, Y. Sun, X. Wang, D. An, Z. Wen, P. Chen, Y. Cheng, The clinical significance of isocitrate dehydrogenase 2 in esophageal squamous cell carcinoma, Am J Cancer Res, 7 (2017) 700-714.

[8] J. Li, Y. He, Z. Tan, J. Lu, L. Li, X. Song, F. Shi, L. Xie, S. You, X. Luo, N. Li, Y. Li, X. Liu, M. Tang, X. Weng, W. Yi, J. Fan, J. Zhou, G. Qiang, S. Qiu, W. Wu, A.M. Bode, Y. Cao, Wild-type IDH2 promotes the Warburg effect and tumor growth through HIF1α in lung cancer, Theranostics, 8 (2018) 4050-4061.

[9] E. Bergaggio, C. Riganti, G. Garaffo, N. Vitale, E. Mereu, C. Bandini, E. Pellegrino, V. Pullano, P. Omedè, K. Todoerti, L. Cascione, V. Audrito, A. Riccio, A. Rossi, F. Bertoni, S. Deaglio, A. Neri, A. Palumbo, R. Piva, IDH2 inhibition enhances proteasome inhibitor responsiveness in hematological malignancies, Blood, 133 (2019) 156-167.

[10] D.J. Urban, N.J. Martinez, M.I. Davis, K.R. Brimacombe, D.M. Cheff, T.D. Lee, M.J. Henderson, S.A. Titus, R. Pragani, J.M. Rohde, L. Liu, Y. Fang, S. Karavadhi, P. Shah, O.W. Lee, A. Wang, A. McIver, H. Zheng, X. Wang, X. Xu, A. Jadhav, A. Simeonov, M. Shen, M.B. Boxer, M.D. Hall, Assessing inhibitors of mutant isocitrate dehydrogenase using a suite of pre-clinical discovery assays, Scientific Reports, 7 (2017) 12758.

[11] A. Noureddine, A. Maestas-Olguin, E.A. Saada, A.E. LaBauve, J.O. Agola, K.E. Baty, T. Howard, J.K. Sabo, C.R.S. Espinoza, J.A. Doudna, J.S. Schoeniger, K.S. Butler, O.A. Negrete, C.J.

Brinker, R.E. Serda, Engineering of monosized lipid-coated mesoporous silica nanoparticles for CRISPR delivery, Acta Biomaterialia, 114 (2020) 358-368.
[12] M. Colilla, B. Gonzáleza, M. Vallet-Regí, Mesoporous silica nanoparticles for the design of smart delivery nanodevices, Biomater. Sci., 1 (2013) 114.
[13] Z. Li, J.C. Barnes, A. Bosoy, J.F. Stoddart, J.I. Zink, Mesoporous silica nanoparticles in biomedical applications, Chem. Soc. Rev., 41 (2012) 2590-2605.
[14] R. Narayan, U.Y. Nayak, A.M. Raichur, S. Garg, Mesoporous Silica Nanoparticles: A Comprehensive Review on Synthesis and Recent Advances, Pharmaceutics, 10 (2018) 118.
[15] C. Argyo, V. Weiss, C. Bräuchle, T. Bein, Multifunctional Mesoporous Silica Nanoparticles as a Universal Platform for Drug Delivery, Chem. Mater., 26 (2014) 435−451.
[16] M.W. Ambrogio, C.R. Thomas, Y.-L. Zhao, J.I. Zink, J.F. Stoddart, Mechanized Silica Nanoparticles: A New Frontier in Theranostic Nanomedicine, Acc. Chem. Res., 44 (2011) 903-913.
[17] V. Cauda, A. Schlossbauer, J. Kecht, A. Zürner, T. Bein, Multiple Core−Shell Functionalized Colloidal Mesoporous Silica Nanoparticles, J. Am. Chem. Soc., 131 (2009) 11361-11370.
[18] V. Cauda, C. Argyo, T. Bein, Impact of different PEGylation patterns on the long-term bio-stability of colloidal mesoporous silica nanoparticles, J. Mater. Chem., 20 (2010) 8693-8699.
[19] J. Simmchen, A. Baeza, D. Ruiz, M.J. Esplandiu, M. Vallet-Regí, Asymmetric Hybrid Silica Nanomotors for Capture and Cargo Transport: Towards a Novel Motion-Based DNA Sensor, Small, 8 (2012) 2053-2059.
[20] V. Cauda, H. Engelke, A. Sauer, D. Arcizet, C. Bräuchle, J. Rädler, T. Bein, Colchicine-Loaded Lipid Bilayer-Coated 50 nm Mesoporous Nanoparticles Efficiently Induce Microtubule Depolymerization upon Cell Uptake, Nano Lett., 10 (2010) 2484-2492.
[21] S. Giri, B.G. Trewyn, M.P. Stellmaker, V.S.Y. Lin, Angew. Chem., Int. Ed. , 44 (2005) 5038.
[22] V. Cauda, A. Schlossbauer, T. Bein, Bio-degradation study of colloidal mesoporous silica nanoparticles: Effect of surface functionalization with organo-silanes and poly(ethylene glycol), Microporous Mesoporous Mater., 132 (2010) 60-71.
[23] P.N. Durfee, Y.-S. Lin, D.R. Dunphy, A.J. Muñiz, K.S. Butler, K.R. Humphrey, A.J. Lokke, J.O. Agola, S.S. Chou, I.M. Chen, W. Wharton, J.L. Townson, C.L. Willman, C.J. Brinker, Mesoporous Silica Nanoparticle-Supported Lipid Bilayers (Protocells) for Active Targeting and Delivery to Individual Leukemia Cells, ACS Nano, 10 (2016) 8325-8345.
[24] A. Schlossbauer, A.M. Sauer, V. Cauda, A. Schmidt, H. Engelke, J. Rädler, U. Rothbauer, K. Zolghadr, C. Bräuchle, T. Bein, Cascaded photoinduced drug delivery to cells from multifunctional core-shell mesoporous silica, Advanced Healthcare Materials, 1 (2012) 316-320.
[25] J. Zhang, Z.-F. Yuan, Y. Wang, W.-H. Chen, G.-F. Luo, S.-X. Cheng, R.-X. Zhuo, X.-Z. Zhang, Multifunctional Envelope-Type Mesoporous Silica Nanoparticles for Tumor-Triggered Targeting Drug Delivery, Journal of the American Chemical Society, 135 (2013) 5068-5073.
[26] J. Lin, Q. Cai, Y. Tang, Y. Xu, Q. Wang, T. Li, H. Xu, S. Wang, K. Fan, Z. Liu, Y. Jin, D. Lin, PEGylated Lipid bilayer coated mesoporous silica nanoparticles for co-delivery of paclitaxel and curcumin: Design, characterization and its cytotoxic effect, International Journal of Pharmaceutics, 536 (2018) 272-282.
[27] Y. Qiu, C. Wu, J. Jiang, Y. Hao, Y. Zhao, J. Xu, T. Yu, P. Ji, Lipid-coated hollow mesoporous silica nanospheres for co-delivery of doxorubicin and paclitaxel: Preparation, sustained release,

cellular uptake and pharmacokinetics, Materials science & engineering. C, Materials for biological applications, 71 (2017) 835-843.
[28] X. Liu, A. Situ, Y. Kang, K.R. Villabroza, Y. Liao, C.H. Chang, T. Donahue, A.E. Nel, H. Meng, Irinotecan Delivery by Lipid-Coated Mesoporous Silica Nanoparticles Shows Improved Efficacy and Safety over Liposomes for Pancreatic Cancer, ACS Nano, 10 (2016) 2702-2715.
[29] H. Xue, Z. Yu, Y. Liu, W. Yuan, T. Yang, J. You, X. He, R.J. Lee, L. Li, C. Xu, Delivery of miR-375 and doxorubicin hydrochloride by lipid-coated hollow mesoporous silica nanoparticles to overcome multiple drug resistance in hepatocellular carcinoma, Int J Nanomedicine, 12 (2017) 5271-5287.
[30] K.S. Butler, P.N. Durfee, C. Theron, C.E. Ashley, E.C. Carnes, C.J. Brinker, Protocells: Modular Mesoporous Silica Nanoparticle-Supported Lipid Bilayers for Drug Delivery, Small, 12 (2016) 2173-2185.
[31] W.-C. Yang, S.-F. Lin, Mechanisms of Drug Resistance in Relapse and Refractory Multiple Myeloma, Biomed Res Int, 2015 (2015) 341430-341430.
[32] V. Pinto, R. Bergantim, H.R. Caires, H. Seca, J.E. Guimarães, M.H. Vasconcelos, Multiple Myeloma: Available Therapies and Causes of Drug Resistance, Cancers, 12 (2020) 407.
[33] B. Dumontel, M. Canta, H. Engelke, A. Chiodoni, L. Racca, A. Ancona, T. Limongi, G. Canavese, V. Cauda, Enhanced biostability and cellular uptake of zinc oxide nanocrystals shielded with a phospholipid bilayer, Journal of Materials Chemistry B, 5 (2017) 8799-8813.
[34] B. Dumontel, F. Susa, T. Limongi, M. Canta, L. Racca, A. Chiodoni, N. Garino, G. Chiabotto, M.L. Centomo, Y. Pignochino, V. Cauda, ZnO nanocrystals shuttled by extracellular vesicles as effective Trojan nano-horses against cancer cells, Nanomedicine, 14 (2019) 2815-2833.
[35] L. Bircher, O.M. Theusinger, S. Locher, P. Eugster, B. Roth-Z'graggen, C.M. Schumacher, J.-D. Studt, W.J. Stark, B. Beck-Schimmer, I.K. Herrmann, Characterization of carbon-coated magnetic nanoparticles using clinical blood coagulation assays: effect of PEG-functionalization and comparison to silica nanoparticles, Journal of Materials Chemistry B, 2 (2014) 3753-3758.
[36] C. Santos, S. Turiel, P. Sousa Gomes, E. Costa, A. Santos-Silva, P. Quadros, J. Duarte, S. Battistuzzo, M.H. Fernandes, Vascular biosafety of commercial hydroxyapatite particles: discrepancy between blood compatibility assays and endothelial cell behavior, Journal of Nanobiotechnology, 16 (2018) 27.
[37] R. Tavano, D. Segat, E. Reddi, J. Kos, M. Rojnik, P. Kocbek, S. Iratni, D. Scheglmann, M. Colucci, I.M.R. Echevarria, F. Selvestrel, F. Mancin, E. Papini, Procoagulant properties of bare and highly PEGylated vinyl-modified silica nanoparticles, 5 (2010) 881-896.
[38] A. Schlossbauer, A.M. Sauer, V. Cauda, A. Schmidt, H. Engelke, J. Rädler, U. Rothbauer, K. Zolghadr, C. Bräuchle, T. Bein, Cascaded photoinduced drug delivery to cells from multifunctional core-shell mesoporous silica, Advanced Healthcare Materials, 1 (2012) 316-320.
[39] A. Ancona, B. Dumontel, N. Garino, B. Demarco, D. Chatzitheodoridou, W. Fazzini, H. Engelke, V. Cauda, Lipid-Coated Zinc Oxide Nanoparticles as Innovative ROS-Generators for Photodynamic Therapy in Cancer Cells, Nanomaterials (Basel, Switzerland), 8 (2018).
[40] E. Chibowski, A. Szcześ, Zeta potential and surface charge of DPPC and DOPC liposomes in the presence of PLC enzyme, Adsorption, 22 (2016) 755-765.

[41] C. Argyo, V. Cauda, H. Engelke, J. Rädler, G. Bein, T. Bein, Heparin-Coated Colloidal Mesoporous Silica Nanoparticles Efficiently Bind to Antithrombin as an Anticoagulant Drug-Delivery System, 18 (2012) 428-432.

23-25, 27-29, 35-41

TABLES

Table 1. Z-Potential measurements of the pristine and lipid-coated MSNs in MilliQ water at room temperature or cell culture medium (RPMI-1640 completed with 10% of Fetal Bovine Serum, FBS) at 37 °C, which is actually the same conditions used to culture the KMS-28 cancer cells.

Sample	**Z-Potential in water (mV)**	**Z-Potential in cell culture medium (mV)**
MSN	26±3	n.a. *
MSN@DOPC	0.8±0.2	-8.1±1.6
MSN@DOPC-DOTAP	32±3	-10±3
MSN@DOPC-chol-DSPE-PEG	29.0±1.3	-6.0±0.9

*This data is not available due to the imminent aggregation and precipitation of the pristine MSN in cell culture media.

Table 2. Amount of drug adsorbed in the MSN (calculated for 1 mg of silica) and remaining after the lipid self-assembly.

Sample	Drug loading amount [μg drug per 1 mg of silica]
MSN	22.2 ± 1.4 μg/mg
Residual amount after lipid self-assembly	
MSN@DOPC	1 ± 1 μg/mg
MSN@DOPC-DOTAP	12 ± 4 μg/mg
MSN@DOPC-chol-DSPE-PEG	21.91 ± 0.05 μg/mg

Table 3. Mithocondria-extracted IDH2 enzymatic activities using AGI-6780 loaded in MSNs@DOPC (100 μg/mL), MSN@DOPC-chol-DSPE-PEG (25 μg/mL) nanoconstructs and referred to the enzymatic activity of empty nanoconstructs counterparts. KMS-28 cells were also treated with 5 μM AGI-6780 as positive control and its value reported to untreated cells. The IDH2 activity was monitored at 6 hours and 24 hours post-treatment.

	% of enzymatic activity with respect to controls		
Time of inhibition assay	AGI-6780 loaded in MSNs@DOPC	AGI-6780 loaded in MSNs@DOPC-chol-DSPE-PEG	Free AGI-6780
After 6 hours	103.57± 0.14	87.32 ± 0.10	50.80 ± 0.11
After 24 hours	47.49 ± 0.08	66.28 ± 0.07	25.65 ± 0.08

FIGURE CAPTIONS

Figure 1. (a) Transmission Electron Microscopy (TEM) and (b) Scanning Transmission Electron Microscopy (STEM) of the mesoporous silica nanoparticles (MSN). Scale bar is 20 nm; (c) Nitrogen sorption isotherms with DFT pore size distribution in the inset; (d) Fourier-Transform infrared Spectroscopy (FTIR).

Figure 2. Particle size distribution measured by dynamic light scattering (DLS), comparing the pristine MSN with MSN coated by the various SLB.

Figure 3. Fluorescence co-localization microscope images of the various lipid-coated MSN. (a-c) MSN@DOPC; (d-f) MSN@DOPC-DOTAP; (g-i) MSN@DOPC-chol-DSPE-PEG. Figures on the left column refer to the emission in the green channel (λ_{ex} = 488 nm); those in the central column to the red channel (λ_{ex} = 550 nm), and the right column refers to the merged channel for colocalization evaluation (yellow indicates colocalization of MSN with lipids). Scale bars are 10 μm.

Figure 4. (a) Drug leakage at 24 hours evaluated in percentage with respect to the total adsorbed drug evaluating the stability of the various nanocostructs (0.5 mg of sample) in water at two different storage temperatures, 4 °C (filled bars) and 37 °C (dashed bars). (b) Release of AGI drug from pristine MSN (in grey) and from two lipid-coated mesoporous silica, i.e. MSN@DOPC-DOTAP (in red), MSN@DOPC-chol-DSPE-PEG (in black). Y-axis reports the percentage of the released drug AGI-6780 in RPMI-1640 with respect to the loaded amount. The inset shows a detail of the drug release from the MSN@SLB only. Error bars are S.E.M.

Figure 5. Results of the haemocompatibility tests comparing samples in citrate plasma and evaluating the coagulation time (t_c) after addition of calcium chloride ($CaCl_2$). The UV-vis absorption at 405 nm is recorded over time for 45 minutes on samples (upper panel): plasma; plasma with physiological

solution (0.9%wt NaCl); pristine MSNs at two concentrations (50 and 100 µg/mL); MSN@DOPC-chol-DSPE-PEG at two concentrations (50 and 100 µg/mL); and the coagulation time recorded, as reported in the table (lower panel).

FIGURES

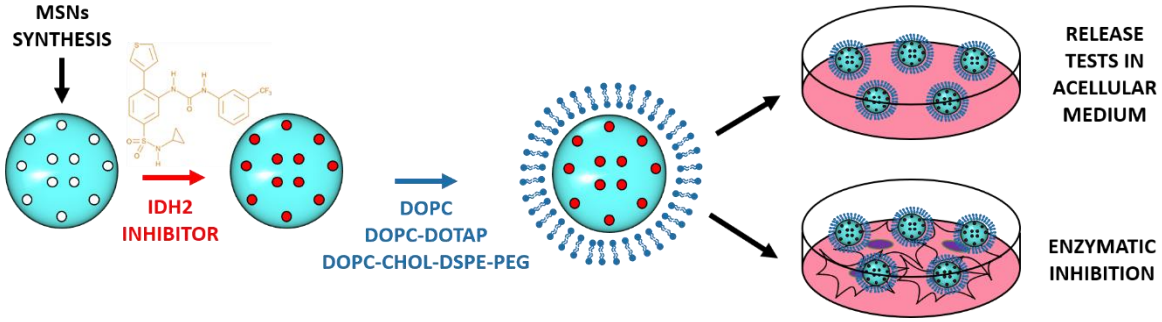

Graphical abstract

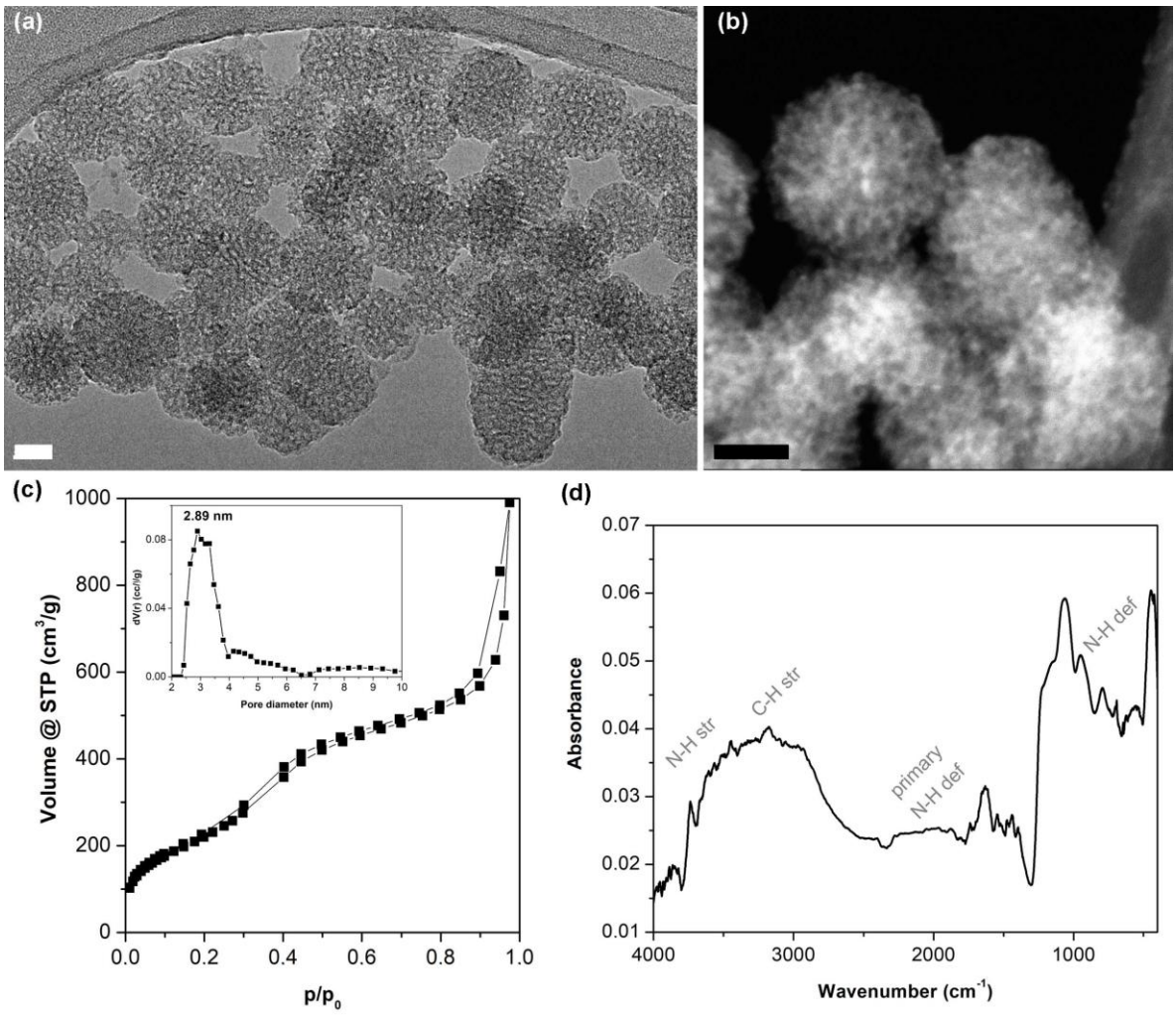

762

763 **Figure 1**

764

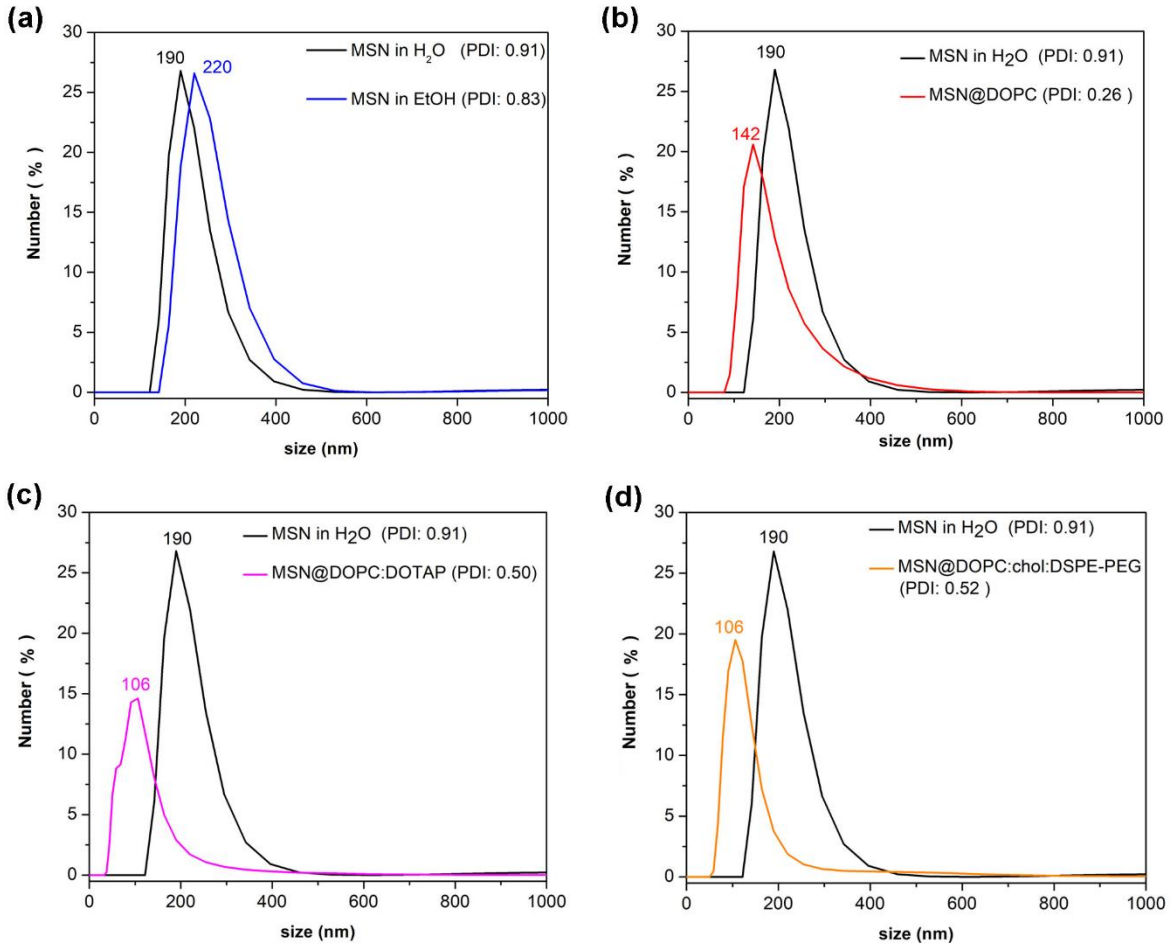

765

766 **Figure 2**

767

768

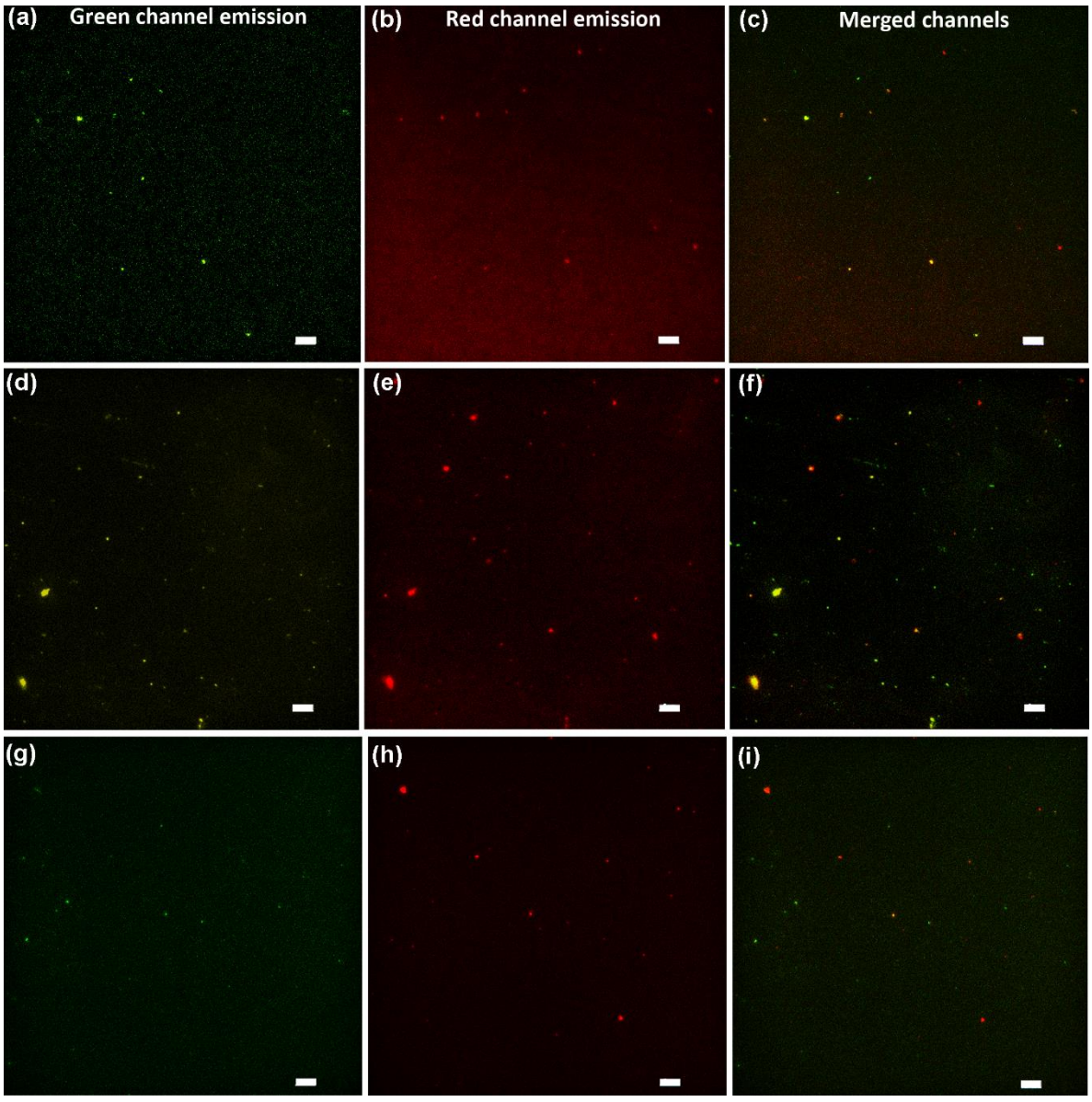

769

770 **Figure 3**

771

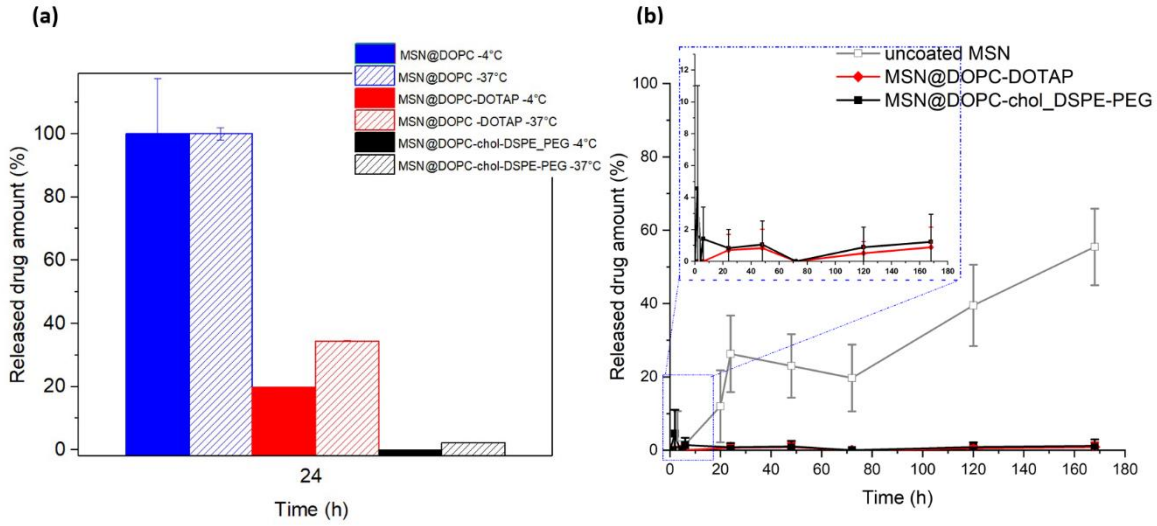

772

773 **Figure 4**

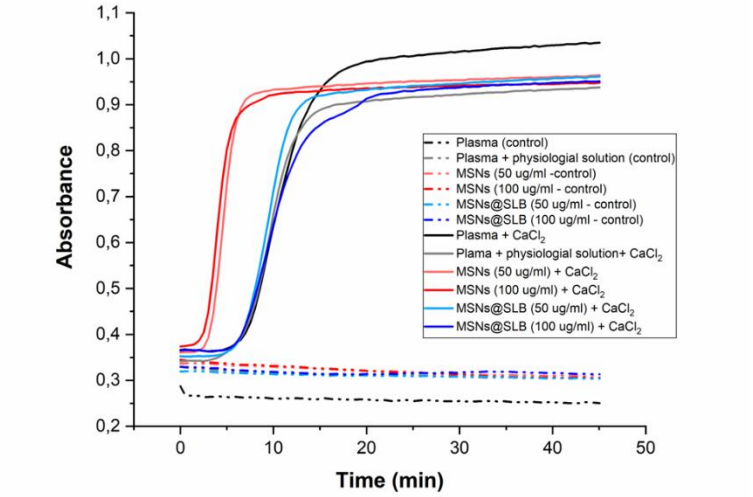

Samples	Average t_c ± st.dev (min)
Plasma	10.2±0.8
Physiological solution	9.6±0.3
MSNs (50 ug/ml)	4.8±0.2
MSNs 100 ug/ml	4.4±0.4
MSNs@DOPC-chol-DSPE-PEG (50 ug/ml)	9.39±0.19
MSNs@DOPC-chol-DSPE-PEG (100 ug/ml)	9.5±1.1

774

775 **Figure 5**

776

777